Modeling Temperature Distribution in Cylindrical Lithium Ion Batteries for Use in Electric Vehicle Cooling System Design

by

Samuel Anthony Jasinski

SUBMITTED TO THE DEPARTMENT OF MECHANICAL ENGINEERING IN PARTIAL FULFILLMENT OF THE REQUIREMENTS FOR THE DEGREE OF

BACHELOR OF SCIENCE IN MECHANICAL ENGINEERING
AT THE
MASSACHUSETTS INSTITUTE OF TECHNOLOGY

JUNE 2008

Signature of Author:_____
Department of Mechanical Engineering
May 9, 2008

Certified by:_____
Yet-Ming Chiang
Professor of Materials Science and Engineering
Thesis Supervisor

Accepted by:_____
John H. Lienhard V
Professor of Mechanical Engineering
Chairman, Undergraduate Thesis Committee

Modeling Temperature Distribution in Cylindrical Lithium Ion Batteries for Use in Electric Vehicle Cooling System Design

by

Samuel Anthony Jasinski

Submitted to the Department of Mechanical Engineering
on May 9, 2008 in partial fulfillment of the
requirements for the Degree of Bachelor of Science in
Mechanical Engineering

ABSTRACT

Recent advancements in lithium ion battery technology have made BEV's a more feasible alternative. However, some safety concerns still exist. While the energy density of lithium ion batteries has all but made them the premier electric vehicle (EV) battery choice, their potential to overheat and explode is a limiting factor. Beyond certain temperature thresholds, lithium ion batteries will experience what is known as thermal runaway. During thermal runaway, the temperature of the battery increases uncontrollably and fires and explosions can occur. For this reason, adequate thermal management is a necessity in bringing lithium ion battery powered vehicles to market.

The purpose of this work is to 1) develop mathematical models for temperature distribution and heat transfer in cylindrical lithium-ion cells and battery packs, 2) derive the target heat transfer coefficient for an EV cooling system 3) analyze the key design parameters of EV thermal management systems, and, ultimately, 4) determine the method of cooling necessary to prevent thermal runaway. The models are based on the fundamentals of heat transfer and are integrated into computer simulations for testing.

Based on the models developed in this analysis, forced convection at the surface of the battery pack is not sufficient for preventing thermal runaway outside of minimum operational requirements (low ambient temperatures and discharge rates). For typical vehicle usage, a system in which the working fluid penetrates the pack is needed. There may be potential for a hybrid cooling system: one that relies on surface convection for less strenuous operation and strategically placed cooling channels for typical and extraneous operation.

Thesis Supervisor: Yet-Ming Chiang
Title: Professor of Materials Science and Engineering

Table of Contents

List of Symbols

A, coefficients matrix

A_{cond}(18mm), cross sectional area of conduction between batteries in pack normalized, $\frac{mm^2}{l}$

A_{conv}(14.14mm), surface area of battery convective surface in pack normalized, mm

$A_{surface}$(0.004mm^2), surface area of batter, mm^2

B_i(5×10^{-5}), Biot number comparing thermal resistance of lumped system to ambient

C, constants matrix

d(18mm), battery diameter, mm

h, convection coefficient from battery surface to ambient, $\frac{W}{m^2 \cdot °C}$

H(0.45m), pack height, m

h_c, critical convection coefficient for preventing thermal runaway, $\frac{W}{m^2 \cdot °C}$

I, current draw, A

I_{cell}, current draw per cell, A

k_{LV}(0.0042), thermal conductivity of lumped system, $\frac{W}{m \cdot °C}$

k_{pack}, thermal conductivity of pack material, $\frac{W}{m \cdot °C}$

k_{steel}(60), thermal conductivity of steel battery enclosure, $\frac{W}{m \cdot °C}$

l(65mm), battery length, mm

L(0.715m), pack length, m

$\dot{q}$, heat generation normalized by battery length, $\frac{W}{mm}$

q_{cond}, conduction between batteries in pack normalized by battery length, $\frac{W}{mm}$

q_{conv}, convection between batteries in pack and ambient normalized by battery length, $\frac{W}{mm}$

$\dot{q}_{gen}$, heat generation per unit volume in lumped system, $\frac{W}{mm^3}$

$\dot{Q}_{gen}$, heat generation in lumped system, W

R_{can}(0.0023), thermal resistance of can, $\frac{W}{°C}$

$R_{convection}$, thermal resistance of convection, $\frac{W}{°C}$

$R_{internal}$(0.01), battery internal resistance, Ω

$R_{thermal}$, thermal resistance in heat transfer circuit, $\frac{W}{°C}$

r_0(0.5mm), radius of battery internal gap, mm

r_s(9mm), radius of battery surface, mm

r_w(8.5mm), radius of enclosure inner wall, mm

T, Temperature column vector

T_0(60°C), thermal runaway threshold temperature, °C

$T_{i,j}$, temperature of node (i,j) in pack nodal network, °C

$T_{surface}$, surface temperature of battery, °C

T_{wall}, temperature at enclosure inner wall, °C

T_∞, temperature of ambient or working fluid, °C

W(0.45m), width of pack, m

ΔT_{cell}, change in temperature from cell center to surface, °C

Introduction

With oil prices sky rocketing and climate change concerns growing, alternative fueled vehicles are at the forefront of the green movement. Car manufacturers are in a tight race to put Hybrid Electric Vehicles (HEV) and Battery Electric Vehicles (BEV) into production. Only a few technical hurdles stand in the way of seeing these clean cars in driveways across the globe. Recent advancements in lithium ion battery technology have made BEV's a more feasible alternative. However, some safety concerns still exist. While the energy density of lithium ion batteries has all but made them the premier BEV battery choice, their potential to overheat and explode is a limiting factor. Beyond certain temperature thresholds, lithium ion batteries will experience what is known as thermal runaway. During thermal runaway, the temperature of the battery increases uncontrollably and fires and explosions can occur. For this reason, adequate thermal management is a necessity in bringing lithium ion battery powered vehicles to market. A well designed cooling system would ensure that the lithium ion batteries in an electric vehicle pack never reached their thermal runaway threshold temperature.

The purpose of this work is to 1) develop mathematical models for temperature distribution and heat transfer in cylindrical lithium-ion cells and battery packs, 2) derive the target heat transfer coefficient for an EV cooling system 3) analyze the key design parameters of EV thermal management systems, and, ultimately, 4) determine the method of cooling necessary to prevent thermal runaway. These models serve as design tools, aiding in the initial stages of cooling system conceptualization. The results provide a starting point for the design process and guide further modeling and testing.

To derive the models, this analysis relies heavily on the fundamentals of heat transfer. Using radial variations of the heat equation for a simplified battery geometry, the cell temperature distribution model is developed. The pack level distribution model is conceived by representing the pack as a nodal network and performing matrix inversion on the system of each node's energy balance equations. For the purposes of this analysis, computer simulations are run varying model inputs. From the simulation results, design implications can be made. The analysis begins at the cell level and works up to the pack level.

1. Cell Level Analysis

1.1 Underlying Principles and Governing Equations: Deriving the Model

Deriving models for heat transfer in batteries is inherently challenging due to the wide range and complexity of battery chemistry and composition. As a result, many assumptions and simplifications must be made. First, because the length of the battery is larger than the diameter, this analysis will focus on heat transfer in the radial direction. Heat transfer along the "y" axis is negligible because of the added thermal resistance. As a result of this assumption, the models derived will be one dimensional. Using batteries that are 18mm in diameter and 65 mm in length, the length to diameter ratio for this analysis is close to 3:1. Second, to simplify further, this analysis will focus on steady state heat transfer. Although idealized, this model acts as a guide for developing more complex, multi-dimensional transient models. The following sections will explain the underlying principles and governing equations of the cell level model.

1.1.1 Internal Geometry Simplification

The first step to deriving a mathematical model for the temperature distribution in a battery is to understand and simplify its internal geometry. Figure 1.1 below illustrates the typical geometry of a cylindrical lithium-ion battery.

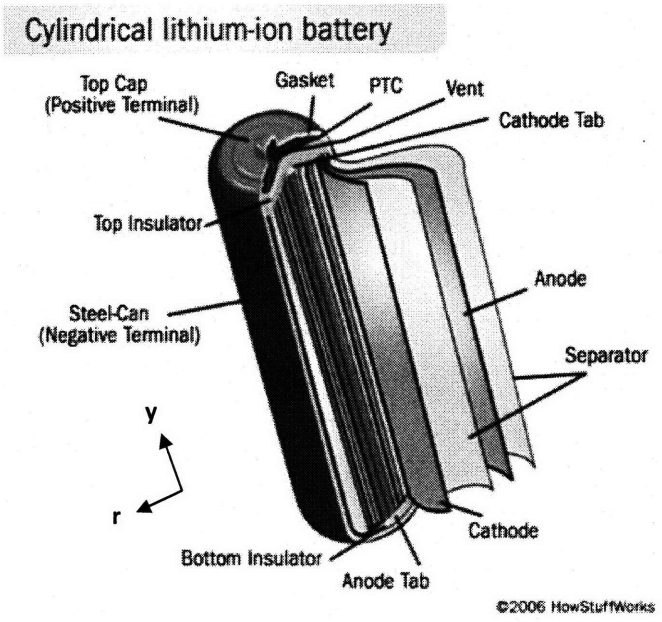

Figure 1.1 Internal Battery Geometry

The heat generation that drives internal battery temperature gradients occurs in the cathode and anode layers. They are separated by another layer which is saturated in the organic carbonate based electrolyte. Comparing the conduction coefficients of the anode, cathode and separator/electrolyte materials reveals that they are all on the same order of magnitude and close to equal [1]. This means each will have equivalent thermal resistances and behave similarly during heat dissipation. As a result, for heat transfer analysis, the internal materials can be modeled as a lumped system having an averaged conduction coefficient. The simplified geometry is represented in Figure 1.2 below.

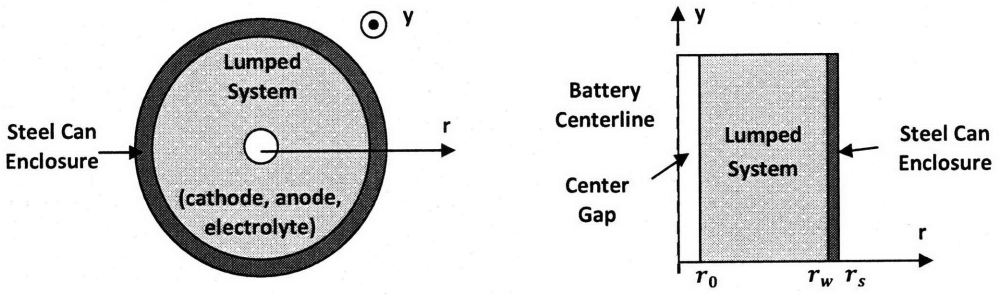

Figure 1.2 Lumped System Simplified Internal Geometry

1.1.2 Internal Heat Generation

Heat generated in a battery is the product of its internal resistance. Internal resistance is an opposition to current flow born from resistivity in the materials of its components and certain electrochemical factors. Electrochemical influences, usually referred to as polarization effects, include electrode conductivity and ion mobility [2]. According to Ohm's Law, the relationship between heat generation, $\dot{Q}_{gen}$, and the battery's internal resistance, $R_{internal}$, is represented by the following equation:

$$\dot{Q}_{gen} = I^2 R_{internal} \tag{1.1}$$

A more complex representation of heat generation would include terms accounting for exothermic entropic effects. However, these effects are only significant at low discharge rates. This analysis is more concerned with the higher discharge rates that correspond to extreme thermal management demands. $R_{internal}$ for this analysis is 0.01 Ω based on battery manufacturers' specifications.

Although heat generation is localized mostly at the anode and cathode, the radial distribution of the electrode layers results in almost uniform generation throughout. Therefore, the heat generation will be estimated as uniform in the simplified lumped system.

1.1.3 Temperature Distribution in Lumped System

To model the temperature distribution in the cylindrical lumped system, the derivation begins with the heat distribution equation. A Fourier's Law derivation, the general form of the heat equation for radial systems is

$$\frac{1}{r}\frac{d}{dr}\left(r\frac{dT}{dr}\right)+\frac{\dot{q}_{gen}}{k_{LV}}=0 \tag{1.2}$$

Here, $\dot{q}_{gen}$ is the heat generated per unit volume in the lumped system and k_{LV} is the conduction coefficient of the lumped volume. This coefficient is an average of the conduction coefficients of the anode, cathode and separator weighted by estimated thickness of each layer. These coefficients and thicknesses are taken from *Srinivasan and Wang*. The resulting lumped coefficient is 0.042 $\frac{W}{mm\cdot K}$. Separating variables and integrating twice results in the general solution for temperature distribution.

$$T(r)=\frac{-\dot{q}_{gen}r^2}{4k_{LV}}+C_1\ln(r)+C_2 \tag{1.3}$$

Applying the following boundary conditions will yield expressions for constants of integration C_1 and C_2.

$$\frac{dT}{dr}|_{r=r_0}=0 \quad and \quad T|_{r=r_1}=T_{wall}$$

The first boundary condition holds true because the center gap with radius, r_0, is surrounded by the lumped volume and remains at a constant temperature. In the second boundary condition, T_{wall} is a common variable linking this temperature distribution equation to the distribution model for the steel enclosure derived later in the following section. Inputting the integration constants based on these boundary conditions into Equation 1.3 results in the temperature distribution equation for the lumped system:

$$T(r)|_{(r_0<r<r_w)}=\frac{\dot{q}_{gen}}{2k_{LV}}\left[r_0^2\ln\left(\frac{r}{r_w}\right)+\frac{r_w^2}{2}-\frac{r^2}{2}\right]+T_{wall} \tag{1.4}$$

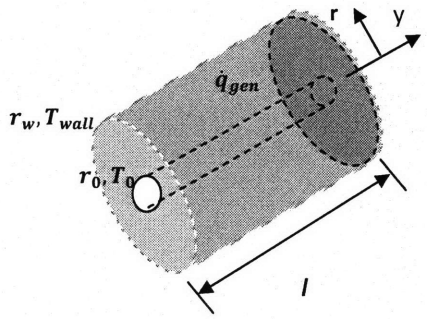

Figure 1.3 Lumped System Cylinder with Uniform Heat Generation

Figure 1.3 above gives a visual representation of the simplified lumped system as a cylinder with uniform heat generation throughout.

1.1.4 Temperature Distribution in Steel Can Enclosure

Next, working outward, a temperature distribution equation is needed for the steel can enclosure of the battery. Using the conduction equation, the heat transfer in the steel can is determined by its thermal resistance and the temperature difference between its inside wall, T_{wall}, and exterior surface, $T_{surface}$.

$$\dot{Q}_{gen} = \frac{T_{wall} - T_{surface}}{R_{thermal}} \tag{1.5}$$

Note that the heat dissipation rate through the steel enclosure is equal to the total heat generation rate, $\dot{Q}_{gen}$, of the lumped volume. The thermal resistance, $R_{thermal}$, of the enclosure is its opposition to the transfer of heat based on the thermal properties of steel. Due to its cylindrical shape, the thermal resistance of the enclosure takes a special form. Accounting for the shape factor, the thermal resistance of the can is

$$R_{can} = \frac{ln\left(\frac{r_s}{r_w}\right)}{k_{steel} 2\pi l} \tag{1.6}$$

Substituting Equation 1.6 for $R_{thermal}$ in Equation 1.5 and setting the resulting expression equal to the general form of Fourier's Law results in the following:

$$\frac{k_{steel} 2\pi l}{ln\left(\frac{r_s}{r_w}\right)} \left(T_{wall} - T_{surface}\right) = k_{steel} 2\pi r l \frac{dT}{dr} \tag{1.7}$$

Separating variables and integrating results in the general form for temperature in the steel can enclosure.

$$T(r) = \frac{T_{wall} - T_{surface}}{ln\left(\frac{r_s}{r_w}\right)} \ln(r) + C_1 \tag{1.8}$$

Using the known boundary condition

$$T|_{r=r_w} = T_{wall},$$

the integration constant is found and the resulting temperature distribution solution for the steel enclosure is

$$T(r)|_{r_w<r<r_s} = \frac{T_{wall} - T_{surface}}{ln\left(\frac{r_s}{r_w}\right)} \ln\left(\frac{r}{r_w}\right) + T_{wall} \tag{1.9}$$

1.1.5 Convection Coefficient

Conducting a similar heat transfer analysis results in an equation for the convection coefficient between the battery surface and the ambient (or working fluid). Again, the derivation begins with Equation 1.5. However, the thermal resistance between the surface and the ambient is different. According to the laws of convection, $R_{convection}$, is determine by the following relationship:

$$R_{convection} = \frac{1}{hA_{surface}} \tag{1.10}$$

Substituting Equation 1.10 for $R_{thermal}$ in Equation 1.5 and solving for h results in

$$h = \frac{\dot{Q}_{gen}}{2\pi r_s l(T_s - T_\infty)} \tag{1.11}$$

where T_∞ is the ambient temperature. Equation 1.11 is the final piece of the overall model that determines the critical convection coefficient necessary to prevent thermal runaway.

1.2 Using the Model to Find the Critical Convection Coefficient

The overall model has three important components; the temperature distribution in the heat generating lumped system, the temperature distribution in the steel can enclosure and the equation for the convection coefficient to the ambient. To combine the three into a continuous model, the first two are used in a slightly different form than derived in the previous section. The temperature distribution in the lumped system becomes

$$T_{wall} = T_o - \frac{\dot{q}_{gen}}{2k_{LV}}\left[r_0^2 \ln\left(\frac{r_0}{r_w}\right) + \frac{r_w^2}{2} - \frac{r_0^2}{2}\right] \tag{1.12}$$

when Equation 1.4 is evaluated at

$$T(r_0) = T_0$$

and the result is solved for T_{wall}. Next, the temperature distribution in the steel enclosure becomes

$$T_{surface} = T_{wall} - \frac{\dot{Q}_{gen} ln\left(\frac{r_s}{r_w}\right)}{2\pi k_{steel} l} \tag{1.13}$$

when Equation 1.9 is solved for $T_{surface}$. The final equation in the overall model, the equation for the target convection coefficient, remains in its original form. Recall Equation 1.11

$$h = \frac{\dot{Q}_{gen}}{2\pi r_s l(T_{surface} - T_\infty)}$$

The model inputs are current draw I, the ambient or working fluid temperature T_∞, and the thermal runaway threshold temperature T_0. The threshold temperature is set at 60°C based on lithium ion battery specifications. This threshold is assumed to already have a safety factor included. The current draw and ambient temperature inputs are varied to analyze their influence on the critical convection coefficient.

First, the current draw is input into Equation 1.1 to derive the corresponding heat generation. Then, this value of $\dot{Q}_{gen}$ is divided by the volume of the lumped system to get $\dot{q}_{gen}$ which is input into Equation 1.12 to derive the corresponding wall temperature. Next, this wall temperature is input into Equation 1.13 to derive the corresponding surface temperature, $T_{surface}$. Finally, this surface temperature and the ambient temperature are input into Equation 1.11 to derive the convective heat coefficient that will keep the internal temperature of the battery below 60°C, thus preventing thermal runaway. The flow chart in Figure 1.4 displays this procedure graphically.

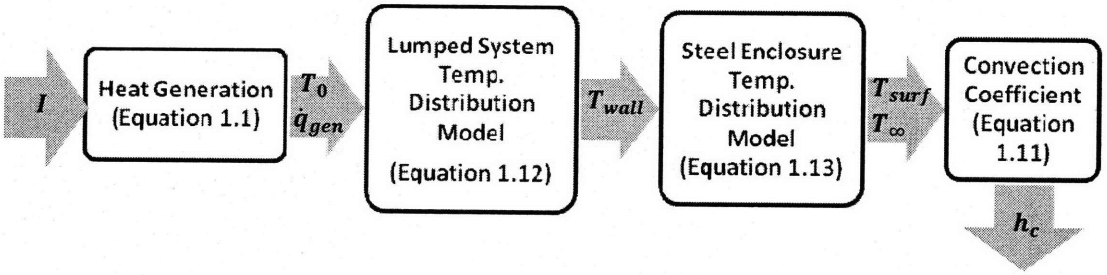

Figure 1.4 Flow Chart of Cell Level Model

Model iterations are easiest to execute using computer simulation. The results of this analysis are generated in Excel. During simulation, the current draw is varied from 10-200A at 10 and 20A intervals. At each amperage, the model is executed with input ambient temperatures of 0, 15, 30 and 40°C. These ranges were chosen to represent the upper and lower bounds of vehicle usage. A draw of 10 amps at 0°C is the equivalent of a vehicle crawling through a parking lot in the winter, not a high risk for thermal runaway. A draw of 200 amps at 40°C is the equivalent of a drag race during the summer in the desert, a high risk of thermal runaway.

1.3 Cell Level Model Results and Implications

The raw data of this analysis can be observed in Appendix A, however, this paper will focus on three major results: the heat generation per cell, $\dot{Q}_{gen}$, the change in temperature throughout the cell, ΔT_{cell}, and, most importantly, the critical convection coefficient, h_c. Heat generation ranged from 1 to 400 W/cell, the temperature change never surpassed 1°C, and a wide range of critical convection coefficients resulted. These values are highlighted due to their influence on the pack level modeling and their implications for cooling system design requirements.

Because heat generation is related to the square of the current draw, it ranged from 1 W/cell at 10A to 400 W/cell at 200A. These values are good approximations, but their validity is inconsistent because they were derived using an average internal resistance. In reality, internal resistance is a function of the state of charge (SOC) and temperature of the battery. A battery's internal resistance is inversely proportional to both [3]. Even so, the values obtained using this analysis' models act as useful guidelines in the design process. While the lower bound of heat generation does not have a significant impact on thermal management design, the upper bound does. Four hundred watts is a lot of heat to dissipate, and a considerable load for a cooling system. Even though a sustained 200A current draw is unlikely, the extremity of the safety consequences necessitates a system that could handle such an event. One way to limit the current draw in each battery is to adopt a system with batteries in series and parallel. Following Kirchhoff's Current Law, the current draw per cell can then be divided by the number

of sets in parallel, in turn reducing the heat generation per cell by a factor of the number of sets squared. This relationship is illustrated below in Figure 1.5.

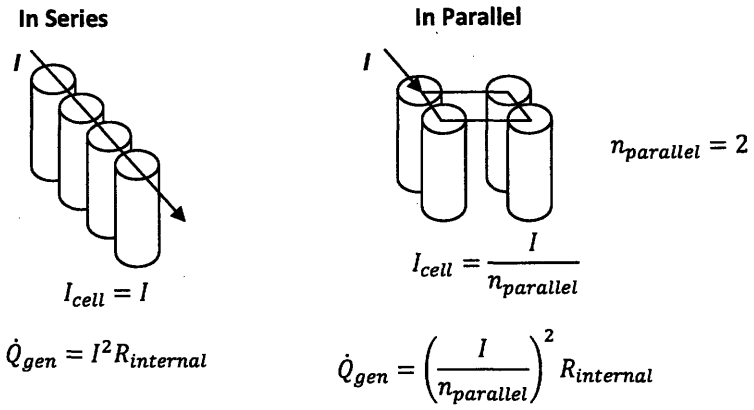

Figure 1.5 Heat Generation Comparison:
Batteries in Series vs. Batteries in Parallel

Putting batteries in parallel to limit current flow will also reduce the voltage drop across the entire system. As a result, more parallel sets of batteries in series will be needed to achieve the desired voltage for the entire pack. This explains the proposed pack designs consisting of thousands of batteries from EV manufacturers, such as Tesla Motors.

The change in temperature within the cell is an important factor in modeling battery interaction at the pack level. This analysis shows that ΔT_{cell} is minimal. Consistently throughout the simulation, there is less than a 1°C temperature difference between the battery center and surface. A simple Biot number analysis validates these results. The Biot number is a dimensionless number relating the thermal resistance of the battery system to the thermal resistance of convection to the ambient.

$$B_i = \frac{R_{can}}{R_{convection}} \tag{1.14}$$

The Biot number for this analysis, assuming a reasonable forced convection coefficient of 100 $\frac{W}{m \cdot K}$, is about 5×10^{-5}. The Biot number being much less than one indicates that the resistance in the battery is negligible in comparison and the temperature within can be modeled as uniform. Other studies have had similar findings using different modeling methodologies [4], [5].

The most important results of the cell level analysis are the values for the critical convection coefficient. This value translates to an imperative thermal management system functional requirement. If the cooling system cannot meet the target convection requirement, thermal runaway and catastrophic accidents could occur. Graphs 1.1 and 1.2 below plot h_c vs. I at the different ambient temperature regimes.

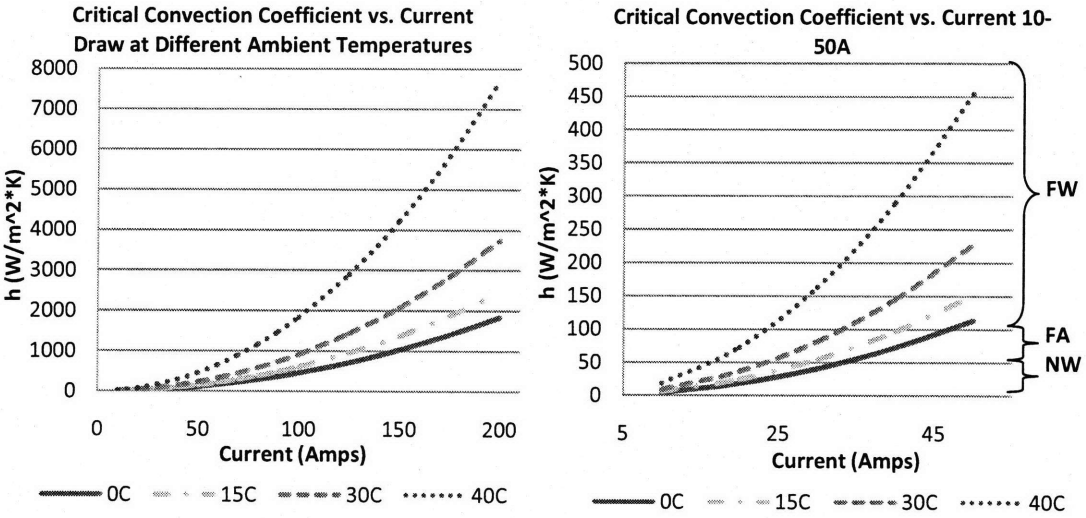

Graphs 1.1 and 1.2

The critical convection coefficient increases as current and ambient temperature increase. Because is proportional to , higher currents drive the curve to resemble the heat generation relationship. Graph 1.2 on the right eliminates the extreme current draw cases, focusing on the discharge currents that are more typical of everyday driving (10-50A). Comparing the results with known convection ranges of possible cooling fluids (air and water), design implications can be made. In all cases, the target convection coefficient was out of the range of natural air convection. Most fell in the range of forced air (FA), forced water (FW) or natural water (NW) convection. These regimes are labeled to the right of Graph 1.2. While there is a range of usage inputs for which forced air convection would be sufficient, typical vehicle usage necessitates convection coefficients in the liquid cooling range. The table below provides the current ranges at each ambient temperature for which either forced air or water convection are appropriate.

Ambient Temperature,	Cooling Method	Current Range (Amps)
0˚C	Forced Air	10-20
	Forced Water	30+
15˚C	Forced Air	10-20
	Forced Water	30+
30˚C	Forced Air	10-
	Forced Water	20+
40˚C	Forced Air	10-
	Forced Water	20+

Table 1.1 Cooling Method Regimes

These results prove the need for a thermal management system with liquid cooling capabilities. In addition, there seems to be the possibility of designing a hybrid cooling system. One that, controlled properly, uses air in some driving instances and liquid in others. To design a hybrid air and liquid cooling system, more detailed models would need to be developed. Increased confidence in the cooling method ranges estimated in Table 1.1 is necessary to ensure a well designed control system. The results and conclusions of the cell level analysis will guide the following derivation of a pack level heat transfer model.

2. Pack Level Analysis

Before developing mathematical models for the temperature distribution and heat transfer in an EV battery pack, a pack design must be established. The geometry and configuration of the model used in this analysis will be based on the battery system in the Tesla Roadster. It consists of 6800 cells at a potential of 375 volts [6]. There are two reasons for choosing to base the models on the Roadster. Most importantly, the Roadster was built for speed and acceleration. These vehicle functional requirements translate to the highest levels of heat generation and, as a result, the most stringent cooling requirements. In addition, the Roadster design uses cylindrical batteries with dimensions identical to those used in the previous cell level analysis.

2.1 Establishing Pack Geometry

The model pack is prismatic in shape. Because space in vehicles is limited, the battery pack is estimated to be limited to a meter in length, a half meter in height and a half meter in width. These limitations result in a pack that is 25 batteries high, 25 batteries wide and 11 batteries long. Within the pack, the batteries are oriented such that the radial heat transfer paths are perpendicular to the larger faces of the pack. This configuration maximizes the convective heat transfer surface for cooling. A scaled down (roughly 1:5) version of this configuration is illustrated in Figure 2.1 below. Note that, due to the size of the actual model (25 batteries X 25 X 11), most operations will be illustrated using scaled down versions or small cross sections.

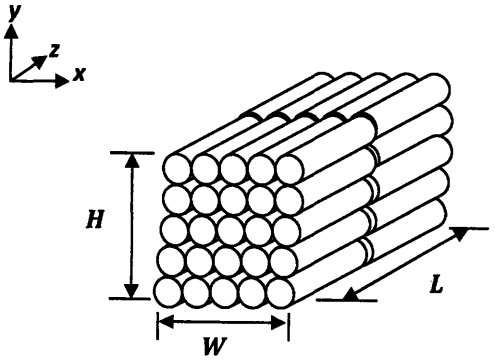

Figure 2.1 Battery Pack Configuration

2.2 The Pack as a Nodal Network

To derive a model for the temperature distribution at the pack level, a different method will be used. Instead of finding an analytical model that determines the temperature anywhere in the system, a numerical model is derived to find the temperature at discrete points. These discrete points will be strategically determined nodes throughout the pack. The conglomeration of these nodes will be the nodal network representing the whole system. Because the pack is considerably longer than it is wide or tall, heat transfer will be modeled in the "x" and "y" directions only. As a result, only a two dimensional network is necessary. If each battery is treated as a node, a small section of the resulting network becomes

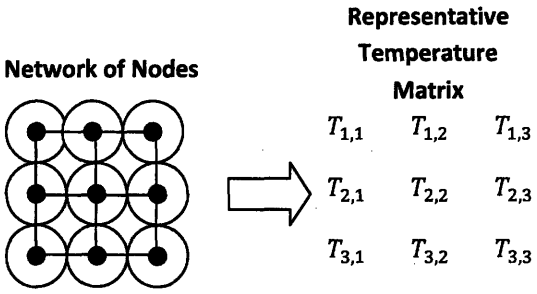

Figure 2.2 Nodal Network of Battery Temperatures

2.3 Nodal Energy Balance

An equation for each node's temperature is derived by applying conservation of energy across a control volume about each node. Two important conventions are applied to each control volume. The first is the inclusion of a heat generation term, $\dot{q}$, representing the heat generated per unit length in each battery. The second is the assumption that heat is dissipating outward in the cardinal directions, and, therefore, each battery interacts only with the batteries to the right, left and above and below it. Under this assumption, heat transfer should be modeled as negative. For the battery pack geometry, there are three variations of this energy balance analysis; the corner case, the wall case and the interior case. Control volume diagrams for each case are displayed in Figure 2.3

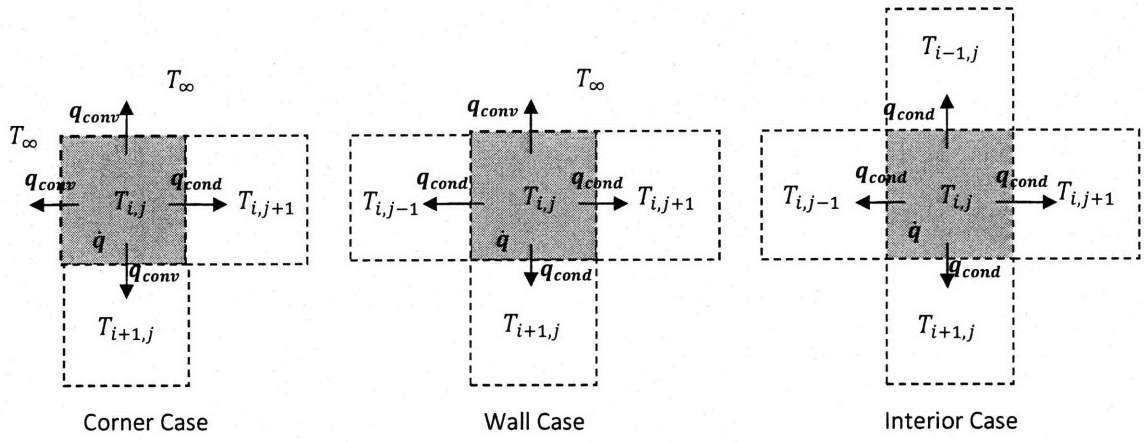

Figure 2.3 Case Specific Energy Balance Diagrams

For each node's control volume the energy balance is

$$\dot{q} + \sum_{out} q = 0 \tag{2.1}$$

According to Fourier's law, the general forms for the convection and conduction dissipation equations are

$$q_{conv} = hA_{conv}(T_{i,j} - T_{i\pm1,j\pm1}) \tag{2.2}$$

$$q_{cond} = \frac{k_{pack}A_{cond}}{t_{cond}}(T_{i,j} - T_{i\pm1,j\pm1}) \tag{2.3}$$

respectively. These general relationships can be made unique to the battery pack model by using the physical system to determine the variables h, k_{pack}, t_{cond}, A_{conv}, and A_{cond}. Modeling the convective surfaces is fairly simple. Because each node is modeled as having four boundaries through which heat can be transferred, the surface area, A_{conv}, is roughly one fourth the surface area of the battery. Therefore,

$$\frac{A_{conv}}{l} = \frac{\pi dl}{4} \tag{2.4}$$

where d is the diameter of the battery and l is eliminated, because the system is being normalized in the "z" direction. The convection coefficient, h, will be a variable input for this

model. Modeling the conduction heat transfer is a little more complicated. Some assumptions are made to simplify the geometry. Figure 2.4 magnifies and simplifies the physical interaction between two batteries within the pack.

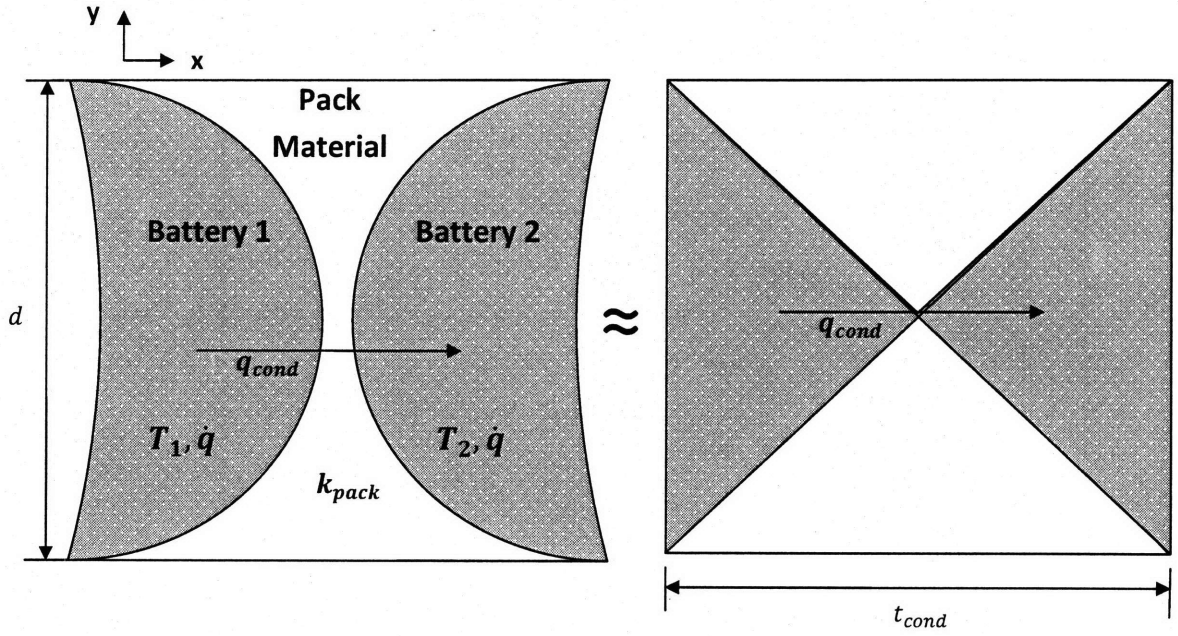

Figure 2.4 Battery Interaction Simplification

Based on the cell level analysis results, the batteries can be modeled as cylinders with uniform temperature. Under this assumption, the only interaction between adjacent batteries is conduction through the pack material that separates them. The cross sectional area of conduction, A_{cond}, normalized in the "z" direction is equal to the diameter of the battery. The conduction thickness, t_{cond},is also equal to the diameter at its maximum. Notice, however, that it changes along the conduction face, decreasing to a minimum at center. The geometry of the intermediate pack material is approximated as two adjoined triangles as illustrated in Figure 2.4 above. Averaging the conduction thickness along the conduction face, t_{cond} is estimated as equaling half the diameter of the battery. The final task in customizing the general conduction equation is choosing an appropriate conduction coefficient, k_{pack}, for the pack material. The choice of pack material will have a significant impact on the characteristics of the system. For this analysis, different materials will be simulated to observe the effect of their thermal conductivities on the maximum temperature in the battery. For constant k_{pack} simulations, a base value of $0.01\frac{W}{mm^{2}.^{\circ}C}$ is used, representing a plastic with increased thermal conductivity. Implementing these unique system parameters into Equations 2.2 and 2.3 results in the following convection and conduction equations unique to the battery pack model:

$$q_{conv} = \frac{h\pi d}{4}(T_{i,j} - T_{i\pm1,j\pm1}) \tag{2.5}$$

$$q_{cond} = \frac{k_{pack}d}{t_{cond}}(T_{i,j} - T_{i\pm1,j\pm1}) \tag{2.6}$$

Conducting an energy balance using Equations 2.5 and 2.6 appropriately in Equation 2.1 results in the three following variations of temperature equations for the node cases. The first is the equation governing the interior nodes which have four conductive faces.

$$4T_{(i,j)} - T_{(i-1,j)} - T_{(i+1,j)} - T_{(i,j+1)} - T_{(i,j-1)} = \frac{\dot{q}t_{cond}}{k_{pack}d} \tag{2.7}$$

The second is the equation governing the wall nodes which have one convective face and three conductive faces.

$$\left(3 + \frac{h\pi t_{cond}}{4k_{pack}}\right)T_{(i,j)} - T_{(i,j-1)} - T_{(i,j+1)} - T_{(i+1,j)} = \frac{\dot{q}t_{cond}}{k_{pack}d} + \left(\frac{h\pi t_{cond}}{4k_{pack}}\right)T_{\infty} \tag{2.8}$$

Third is the equation governing the corner nodes which have two convective faces and two conductive faces.

$$\left(\frac{h\pi d}{2} + \frac{2k_{pack}d}{t_{cond}}\right)T_{(i,j)} - \left(\frac{k_{pack}d}{t_{cond}}\right)T_{(i,j+1)} - \left(\frac{k_{pack}d}{t_{cond}}\right)T_{(i+1,j)} = \dot{q} + \frac{h\pi d}{2}T_{\infty} \tag{2.9}$$

Applying these equations to each node in the network according to case results in a system of 625 linear, algebraic equations, one for each unknown battery temperature.

2.4 Solving the System with Matrix Inversion

To solve this large system, this analysis uses the method of matrix inversion. The system can be expressed in the general form

$$\begin{aligned} a_{11}T_1 + a_{12}T_2 + a_{13}T_3 + \cdots + a_{1n}T_n &= C_1 \\ a_{21}T_1 + a_{22}T_2 + a_{23}T_3 + \cdots + a_{2n}T_n &= C_2 \\ \vdots \quad \vdots \quad \vdots \quad \vdots \quad \vdots \quad \vdots \\ a_{n1}T_1 + T_{n,2} + a_{n3}T_3 + \cdots + a_nT_{1n} &= C_n \end{aligned} \tag{2.10}$$

in which each temperature is now referred to by a single integer subscript (see Figure 2.2). For the pack model, n is equal to 625. The quantities a_{11} through a_{nn}, and C_1through C_n are the coefficients and constants from the case Equations (2.7 through 2.9). In matrix notation the system of equations is expressed as

$$[A][T] = [C] \tag{2.11}$$

where A is the $n \times n$ matrix of coefficients, T is the column vector of unknown temperatures, and C is the column vector of constants.

$$A = \begin{bmatrix} a_{11} & \cdots & a_{1n} \\ \vdots & \ddots & \vdots \\ a_{n1} & \cdots & a_{nn} \end{bmatrix} \quad T = \begin{bmatrix} T_1 \\ \vdots \\ T_n \end{bmatrix} \quad C = \begin{bmatrix} C_1 \\ \vdots \\ C_n \end{bmatrix} \tag{2.12}$$

The following matrix operation

$$[T] = [A]^{-1}[C] \tag{2.13}$$

will yield a solution vector of values for each of the unknown node temperatures. Mapping these solutions onto the node network gives the temperature distribution in the EV battery pack.

2.5 Battery Pack Simulation

Because the system of equations representing the EV battery pack is so large, computer simulation is needed to manipulate the model. For the purposes of this analysis, the model is integrated into a MATLAB function. The explanation of this integration and the MATLAB script are included in Appendix B. The function 1) takes inputs of current draw I, working fluid temperature T_∞, and convection coefficient h, 2) populates the coefficient and constants matrices according to the energy balance equations and 3) returns the solution vector and

maximum temperature in the pack. This analysis uses the model to determine how pack convection coefficient, working fluid temperature, and pack material thermal conductivity affect the maximum temperature in the pack at different discharge currents. The maximum temperature in the battery pack will always be in the centermost battery.

2.5.1 Impact of Convection Coefficient and Working Fluid Temperature

Determining the effect of the convection coefficient on the maximum internal pack temperature is important in guiding the thermal management design process. Most importantly, this analysis determines whether or not convective cooling solely at the surfaces of the pack is sufficient for preventing thermal runaway. To make this determination, h values representing forced or natural convection of air or water are input using working fluids of 0°C and 20°C at currents from 10-70 A. These working fluid temperatures represent a system using air or liquid at a pre-cooled temperature (0°C) or a typical environmental temperature (20°C). These simulations consistently resulted in maximum temperature changes of less than 0.1°C, even as h reaches 1000 $\frac{W}{m^2 \cdot °C}$. Table 2.1 displays a sample of these results.

$T_\infty = 0$°C		$T_\infty = 20$°C	
$h\left(\frac{W}{m^2 \cdot °C}\right)$	T_{max}(°C)	$h\left(\frac{W}{m^2 \cdot °C}\right)$	T_{max}(°C)
3	130.4011	**3**	150.4011
30	130.3912	**30**	150.3912
100	130.3904	**100**	150.3904
300	130.3902	**300**	150.3902
1,000	130.3901	**1,000**	150.3901
5,000	130.3901	**5,000**	150.3901
10,000	130.3901	**1,0000**	150.3901

Table 2.1 Convection Coefficient Effects on Maximum Temperature

The physical explanation for this is that the optimum result of convective cooling only at the surface is getting the temperature of the outermost batteries to equal the temperature of the working fluid. Because the temperature of each battery is dependent on the temperature of the batteries surrounding it, the layer interacting with the outermost batteries show small decreases in temperature. However, this effect diminishes with depth, leaving the temperature of the center battery insignificantly impacted. As a result, lowering the temperature of the working fluid is more effective than increasing the convection coefficient. However, even with a current draw of 15A, a working fluid at 0°C, and a convection coefficient of 1000 $\frac{W}{m^2 \cdot °C}$, the maximum temperature reaches 73°C, ten degrees above the thermal runaway threshold temperature. This data implicates that in order for a thermal management system relying solely on convection on the outermost pack surfaces to prevent thermal runaway, working fluid temperatures will have to be extremely low. In order to achieve this, the outermost batteries would have to operate at temperatures well outside of their rated ranges.

2.5.2 Impact of Pack Material Thermal Properties

The choice of pack material will have a significant impact on the ability of the system to dissipate heat. The ideal material is one that is dielectric with a high thermal conductivity. A dielectric pack material is imperative to prevent short circuiting. The batteries should only be connected via controllable electric paths with built in safety mechanisms. In addition, the higher the thermal conductivity of the material, the less strain on the thermal management system. Balancing these functional requirements, the best candidate for EV pack material is a newly developed thermal conducting plastic. These plastics currently have thermal conductivities ranging from 1-10 $\frac{W}{m\cdot°C}$ with the possibility of reaching thermal conductivities mirroring metals. Metals should be avoided due to their electric conductivity and density. Electric conductivity increases the risk of short circuiting and density translates to heavier packs, hurting vehicle performance.

To gauge the importance of the thermal properties of the pack material in designing a thermal management system, simulations for k_{pack} conductivities ranging from 0.3 to 50 $\frac{W}{m\cdot°C}$ are run. This range covers traditional plastics, such as LDP, up to future super conductive polymers. Table 2.2 below outlines the operational parameters of each case used in analyzing the effects of altering k_{pack}.

	Case 1	**Case 2**	**Case 3**
$\boldsymbol{I\ (Amps)}$	10	15	20
$\boldsymbol{T_\infty}$(°C)	10	20	40
$\boldsymbol{h\left(\frac{W}{m^2°C}\right)}$	100	100	100

Table 2.2 Operational Case Parameters

Graph 2.1 plots the maximum temperature in the pack vs. the pack material thermal conductivity for different vehicle operation cases.

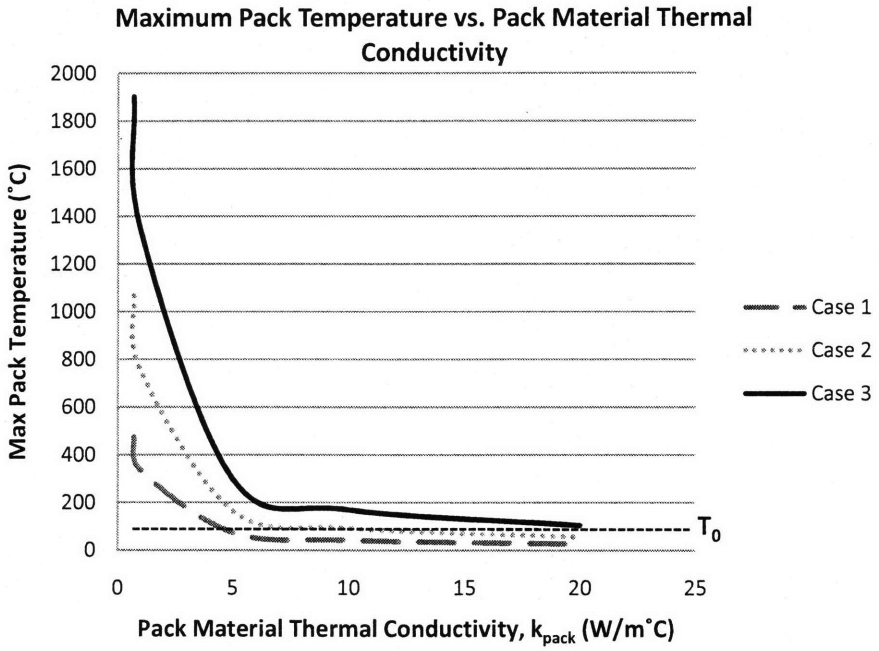

Graph 2.1

The results show that the maximum temperature and thermal conductivity of the pack share the following relationship:

$$T_{max} \sim \frac{1}{k_{pack}}$$

This proves that pack material selection is an important part of the design process. It has the potential to significantly impact the performance of the thermal management system. However, even using thermally conductive plastics in the $10 \frac{W}{m°C}$ range, the pack reaches the thermal runaway threshold in moderate (Case2) and extreme (Case 3) operational cases. In the future, should the thermal conductivities of these experimental polymers reach beyond the 15-$10 \frac{W}{m°C}$ point, convective cooling at the surfaces may become a viable solution. Until then, thermal management systems must penetrate the pack in order to dissipate enough heat to prevent thermal runaway.

3. Conclusion

The large lithium-ion battery packs needed to generate enough power for use in electric vehicles are not conducive to heat dissipation. Without a well designed thermal management system, battery temperatures will surely break the thermal runaway threshold, and catastrophic accidents could occur. Based on the models developed in this analysis, forced convection at the surface of the battery pack is not sufficient for preventing thermal runaway outside of minimum operational requirements (low ambient temperatures and discharge rates). For typical vehicle usage, a system in which the working fluid penetrates the pack is needed. There may be potential for a hybrid cooling system: one that relies on surface convection for less strenuous operation and strategically placed cooling channels for typical and extraneous operation. Based on the critical convection coefficients obtained in the cell level analysis, the working fluid will most likely be liquid.

Further analysis via modeling and testing is necessary to determine the detailed design of a thermal management system. Multi-dimensional, transient models are needed to analyze vehicle acceleration and deceleration effects. In addition, testing should be performed at both the cell and pack levels to validate all models and gather empirical data.

Appendix A Cell Level Results

Table A.1

I (Amps)	$\dot{Q}_{gen}$ (Watts)	$\dot{q}_{gen}$ ($\frac{Watts}{m^3}$)	T_w(°C)	T_s	T_∞	h_c ($\frac{Watts}{m^{2\cdot}{}^\circ C}$)	
10	1	6.04884E-05	59.99999	59.99766	0	4.534505696	**Forced Air**
10	1	6.04884E-05	59.99999	59.99766	15	6.046086192	
10	1	6.04884E-05	59.99999	59.99766	30	9.069365087	
10	1	6.04884E-05	59.99999	59.99766	45	18.14014512	
20	4	0.000241954	59.99997	59.99064	0	18.14014512	
20	4	0.000241954	59.99997	59.99064	15	24.18811805	
20	4	0.000241954	59.99997	59.99064	30	36.28595133	**Water Free**
20	4	0.000241954	59.99997	59.99064	45	72.59455766	
30	9	0.000544395	59.99993	59.97894	0	40.82328774	
30	9	0.000544395	59.99993	59.97894	15	54.4374213	
30	9	0.000544395	59.99993	59.97894	30	81.67525157	
30	9	0.000544395	59.99993	59.97894	45	163.4653284	**Forced Water**
40	16	0.000967814	59.99988	59.96256	0	72.59455766	
40	16	0.000967814	59.99988	59.96256	15	96.81289179	
40	16	0.000967814	59.99988	59.96256	30	145.2798202	
40	16	0.000967814	59.99988	59.96256	45	290.9231408	
50	25	0.00151221	59.99982	59.9415	0	113.468846	
50	25	0.00151221	59.99982	59.9415	15	151.3410251	
50	25	0.00151221	59.99982	59.9415	30	227.1593731	
50	25	0.00151221	59.99982	59.9415	45	455.2080742	
60	36	0.002177582	59.99974	59.91577	0	163.4653284	
60	36	0.002177582	59.99974	59.91577	15	218.0559578	
60	36	0.002177582	59.99974	59.91577	30	327.3909278	
60	36	0.002177582	59.99974	59.91577	45	656.6307377	
70	49	0.002963931	59.99964	59.88535	0	222.6074876	
70	49	0.002963931	59.99964	59.88535	15	296.9995211	
70	49	0.002963931	59.99964	59.88535	30	446.0689855	

I (Amps)	$\dot{Q}_{gen}$ (Watts)	$\dot{q}_{gen}$ ($\frac{Watts}{m^3}$)	T_w(°C)	T_s	T_∞	h_c ($\frac{Watts}{m^2 \cdot °C}$)
70	49	0.002963931	59.99964	59.88535	45	895.5737462
80	64	0.003871257	59.99954	59.85025	0	290.9231408
80	64	0.003871257	59.99954	59.85025	15	388.2213069
80	64	0.003871257	59.99954	59.85025	30	583.305754
80	64	0.003871257	59.99954	59.85025	45	1172.493549
90	81	0.004899559	59.99941	59.81047	0	368.4444729
90	81	0.004899559	59.99941	59.81047	15	491.778745
90	81	0.004899559	59.99941	59.81047	30	739.2314147
90	81	0.004899559	59.99941	59.81047	45	1487.922633
100	100	0.006048838	59.99927	59.76602	0	455.2080742
100	100	0.006048838	59.99927	59.76602	15	607.7371951
100	100	0.006048838	59.99927	59.76602	30	913.9944327
100	100	0.006048838	59.99927	59.76602	45	1842.472109
125	156.25	0.00945131	59.99887	59.6344	0	712.8324048
125	156.25	0.00945131	59.99887	59.6344	15	952.3894721
125	156.25	0.00945131	59.99887	59.6344	30	1434.459022
125	156.25	0.00945131	59.99887	59.6344	45	2904.753988
150	225	0.013609886	59.99837	59.47354	0	1029.255079
150	225	0.013609886	59.99837	59.47354	15	1376.401434
150	225	0.013609886	59.99837	59.47354	30	2076.894957
150	225	0.013609886	59.99837	59.47354	45	4229.335309
175	306.25	0.018524567	59.99778	59.28342	0	1405.423067
175	306.25	0.018524567	59.99778	59.28342	15	1881.478071
175	306.25	0.018524567	59.99778	59.28342	30	2845.237302
175	306.25	0.018524567	59.99778	59.28342	45	5833.215313
200	400	0.024195353	59.9971	59.06407	0	1842.472109
200	400	0.024195353	59.9971	59.06407	15	2469.674377
200	400	0.024195353	59.9971	59.06407	30	3744.276379
200	400	0.024195353	59.9971	59.06407	45	7737.726706

Appendix B Pack Level MATLAB Function

The symmetrical nature of the nodal network allowed for a significant reduction in the number of equations necessary to characterize the temperature distribution in the entire pack. Figure X displays the axes of symmetry. In all, there are only ninety one unique temperatures in the entire system in steady state. Simplification by symmetry did, however, create new variations of the basic case equations. They are listed below.

Exterior Nodes

Variation 1: Corner Case

$$\left(\frac{h\pi d}{2}+\frac{2kd}{t_{cond}}\right)T_{(i,j)}-\left(\frac{2kd}{t_{cond}}\right)T_{(i,j+1)}=\dot{q}+\frac{h\pi d}{2}T_{\infty} \tag{A.1}$$

Variation 2: Inner Wall

$$\left(3+\frac{h\pi t_{cond}}{4k}\right)T_{(i,j)}-T_{(i,j-1)}-T_{(i,j+1)}-T_{(i+1,j)}=\frac{\dot{q}t_{cond}}{kd}+\left(\frac{h\pi t_{cond}}{4k}\right)T_{\infty} \tag{A.2}$$

Variation 3: Inner Wall on Axis

$$\left(3+\frac{h\pi t_{cond}}{4kd}\right)T_{(i,j)}-2T_{(i,j-1)}-T_{(i+1,j)}=\frac{\dot{q}t_{cond}}{kd}+\left(\frac{h\pi t_{cond}}{4k}\right)T_{\infty} \tag{A.3}$$

Interior Nodes

Variation 1: Interior Diagonal Axis (i=j from 2, 2: 12, 12)

$$4T_{(i,j)}-2T_{(i,j+1)}-2T_{(i-1,j)}=\frac{\dot{q}t_{cond}}{kd} \tag{A.5}$$

Variation 2: Interior Vertical Axis

$$4T_{(i,j)}-2T_{(i,j-1)}-T_{(i-1,j)}-T_{(i+1,j)}=\frac{\dot{q}t_{cond}}{kd} \tag{A.6}$$

Variation 3: Midpoint

$$4T_{(i,j)}-4T_{(i-1,j)}=\frac{\dot{q}t_{cond}}{kd} \tag{A.7}$$

Variation 4: Pure Interior

$$4T_{(i,j)}-T_{(i-1,j)}-T_{(i+1,j)}-T_{(i,j+1)}-T_{(i,j-1)}=\frac{\dot{q}t_{cond}}{kd} \tag{A.8}$$

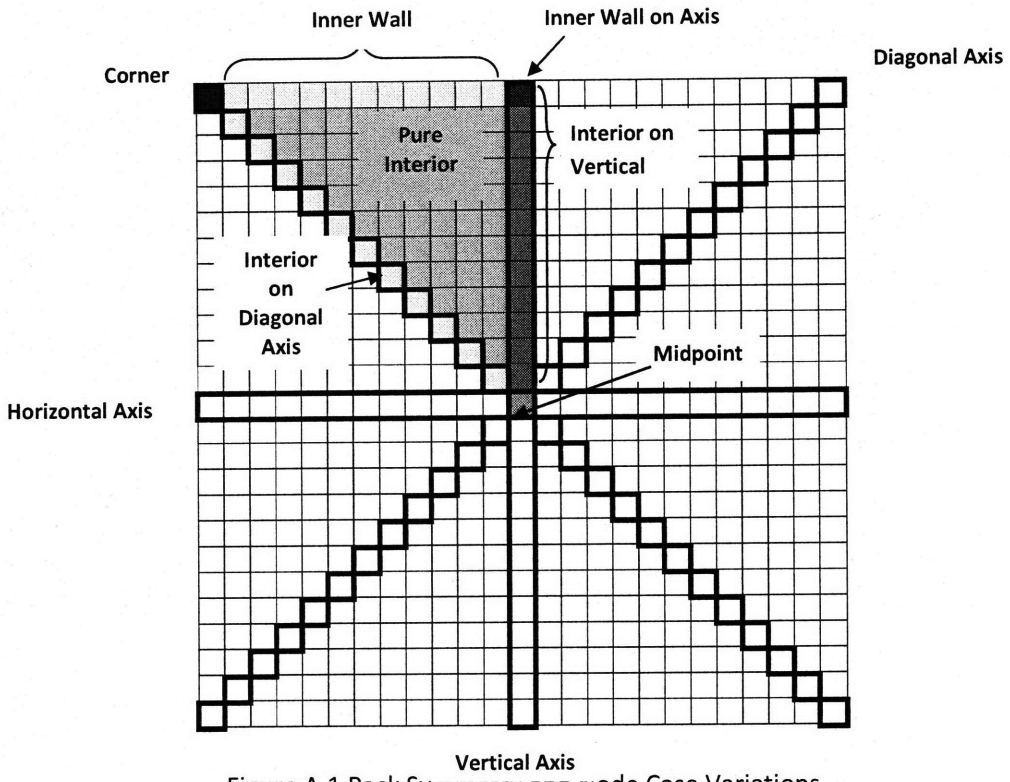

Figure A.1 Pack Symmetry and Node Case Variations

The script of the M-File is copied below. Constants are initialized and the matrices are built by looping through the network indices and implementing the equation cases using conditional statements.

```
function [maxtemp,P]= packtemp(I,Tamb,h)

Rint=0.01;
qdot=(I^2*Rint)/65; %heat generated per unit length
tcond=9;  % conduction thickness (delta x)
d=18;   % conduction distance (= to battery diameter)
k=.01;  % conduction coefficient of pack material

A = zeros (91,91); % Initializes sparse coefficients matrix
j = 14; % diagonal counter
o=14;
n=12;  %axis counter
e=12;
a=12;  % interior counter "a"bove node
b=11;  % interior counter "b"elow node
m=25;  % vertical axis counter
f=25;
```

```
% Building A Matrix
for i = 1:1:91;
    if i ==1
        A(i,1) = ((h*pi*d)/2)+((2*k*d)/tcond);
        A(i,2) = -((2*k*d)/tcond);
    end
    if i >1 && i< 13
        A(i,i) = 3 + (h*pi*tcond)/(4*k);
        A(i,i-1) = -1;
        A(i,i+1) = -1;
        A(i,i+12) = -1;
    end
    if i == 13
        A(i,i) = 3 + (h*pi*tcond)/(4*k);
        A(i,i-1) = -2;
        A(i,i+12) = -1;
    end
    if i == j && i<91
        A(i,i) = 4;
        A(i,i+1)=-2;
        A(i,i-n)=-2;
        j=j+n;
    end
    if i == m && i <91
        A(i,i)=4;
        A(i,i-1)=-2;
        A(i,i-n)=-1;
        n=n-1;
        m=m+n;
        A(i,i+n)=-1;
        a=a-1;
        b=b-1;
    end
    if i>14 && i< 25 || i>26 && i<36 || i>37 && i<46 || i>47 && i<55 || i>56
&& i<63 || i>64 && i<70 || i>71 && i< 76 || i>77 && i<81 || i>82 && i<85 ||
i>86 && i<88
        A(i,i)=4;
        A(i,i+1)=-1;
        A(i,i-1)=-1;
        A(i,i+b)=-1;
        A(i,i-a)=-1;
    end
    if i== 91
        A(i,i)=4;
        A(i,90)=-4;
    end
 end
```

```
% Building C Matrix

C=zeros(91,1);

for i=1:1:91;
    if i==1
        C(i,1)= qdot+((h*pi*d)/2)*Tamb;
    end
    if i>1 && i<13
        C(i,1)=(qdot*tcond)/(k*d)+((h*pi*tcond)/(4*k))*Tamb;
    end
    if i==13
        C(13,1)=(qdot*tcond)/(k*d)+((h*pi*tcond)/(4*k))*Tamb;
    end
    if i>14 && i< 25 || i>26 && i<36 || i>37 && i<46 || i>47 && i<55 || i>56
&& i<63 || i>64 && i<70 || i>71 && i< 76 || i>77 && i<81 || i>82 && i<85 ||
i>86 && i<88
        C(i,1)=(qdot*tcond)/(k*d);
    end
    if i==o
        C(i,1)=(qdot*tcond)/(k*d);
        o=o+e;
    end
    if i==f
        C(i,1)=(qdot*tcond)/(k*d);
        e=e-1;
        f=f+e;
    end
    if i==91
        C(i,1)=(qdot*tcond)/(k*d);
    end
end


P=A\C;
maxtemp=P(91,1);
disp(P);
```

References

1. Srinivasan, V. and Wang, C.Y., 2003, Analysis of Electrochemical and Thermal Behavior of Li-Ion Cells, *Journal of The Electrochemical Society,* v. 150, p. A98- A106.

2. 2005, Battery Internal Resistance, *Energizer Technical Bulletin Version 1.1.0,* http://data.energizer.com/PDFs/BatteryIR.pdf (March 2008).

3. Buchmann, I, How does the internal resistance affect performance? (BU17), *BatteryUniversity.com,* http://batteryuniversity.com/parttwo.htm (April 2008).

4. Chen, Y. and Evans, J.W., 1993, Heat Transfer Phenomena in Lithium/Polymer-Electrolyte Batteries for Electric Vehicle Application, *Journal of The Electrochemical Society,* v.140, p. 1833-1836.

5. Hatchard, T.D., MacNeil, D.D., Basu, A., and Dahn, J.R., 2001, Thermal Model of Cylindrical and Prismatic Lithium-Ion Cells, *Journal of The Electrochemical Society,* v. 148, p. A755-A761.

6. Berdichevsky, G., Kelty, K., Straubel, J.B., and Toomre, Erik, 2006, The Tesla Roadster Battery System, http://www.teslamotors.com/display_data/TeslaRoadsterBatterySystem.pdf (February 2008)

7. Incropera, F.P. and DeWitt, D.P., 1996, *Fundamentals of Heat and Mass Transfer,* John Wiley & Sons, New York City.